Precursors for Waves in Random Media

Guillame Bal[a], Olivier Pinaud[b], Lenya Ryzhik[c], Knut Sølna[d]

[a]*Dept. of Applied Physics & Applied Mathematics, Columbia University, New York, NY 10027, USA* gb2300@columbia.edu .
[b]*Department of Mathematics, Colorado State University, Fort Collins, CO 80523, USA* pinaud@math.colostate.edu.
[c]*Department of Mathematics, Stanford University, Stanford CA 94305, USA* ryzhik@math.stanford.edu.
[d]*Department of Mathematics, University of California at Irvine, Irvine, CA 92697-3875, USA* ksolna@math.uci.edu.

Abstract

We consider scattering of a pulse propagating through a three-dimensional random media and study the shape of the pulse in the parabolic approximation. We show that, similarly to the one-dimensional O'Doherty-Anstey theory, the pulse undergoes a deterministic broadening. Its amplitude decays only algebraically and not exponentially in time, due to the signal low/midrange frequency component. We also argue that the parabolic approximation captures the front evolution (but not the signal away from the front) correctly even in the fully three-dimensional situation.

Keywords: Parabolic approximation, random media, precursor, O'Doherty-Anstey approximation

1. Introduction

The problem of imaging in heterogeneous environments arises in many important applications such as biomedical imaging, telecommunications, seismic exploration in geophysics or non-destructive testing of materials. One standard technique consists in probing a medium with e.g. an electromagnetic pulse and by collecting the echos on an array of detectors. How well the method will perform strongly depends on the structure of the wavefield that propagates in the complex medium. In particular, if the target to be imaged is buried deeply into the medium, scattering effects are important and the measured wavefield might not be strong enough to be used in the inversion.

The main objectives of this work are to determine the spreading and decay of the pulse amplitude in the medium, and to characterize the optimal frequency content of the source in order to probe at a given depth. We will for this consider acoustic waves and model the complex medium by a random medium with appropriate statistics. The propagation of the waves will be described in the parabolic approximation [14] where the complex amplitude of the pressure is solution to a stochastic Schrödinger equation. More precisely, we consider the scalar wave equation in a random medium

$$\frac{1}{c^2(\vec{X})}\frac{\partial^2 u}{\partial T^2} - \triangle u = 0 \ , \quad T > 0 \ , \quad \vec{X} = (X, Z) \in \mathbb{R}^{d+1} \ , \tag{1}$$

with $d = 1, 2$ and the local wave speed $c(X, Z)$ of the form

$$c^{-2}(X, Z) = c_0^{-2} \left[1 + \sigma_0 \mu \left(\frac{X}{l}, \frac{Z}{l} \right) \right] .$$

Here, c_0 is a constant reference speed, $Z \in \mathbb{R}^+$ and $X \in \mathbb{R}^d$ are, respectively, the coordinates along and transverse to the direction of propagation. The random function μ models fluctuations with amplitude σ_0 and correlation length l in the propagation speed. Solutions of the wave equation (1) may be written in the form

$$u(T, X, Z) = \frac{1}{2\pi} \int e^{i\omega(Z/c_0 - T)} \psi \left(Z, X; \frac{\omega}{c_0} \right) d\omega \,, \tag{2}$$

where the complex amplitude $\psi(Z, X; k = K)$ satisfies the Helmholtz equation

$$2iK \frac{\partial \psi}{\partial Z} + \Delta_X \psi + K^2 (n^2 - 1)\psi = -\frac{\partial^2 \psi}{\partial Z} \,. \tag{3}$$

Here $K = \omega / c_0$ is the wavenumber and $n(X, Z) = c_0 / c(X, Z)$ is the random index of refraction relative to c_0. The fluctuations of the refraction index have the form

$$n^2(X, Z) - 1 = \sigma_0 \mu \left(\frac{X}{l}, \frac{Z}{l} \right) .$$

The normalized and dimensionless covariance is given by

$$\tilde{R}(X, Z) = \mathbb{E}\{\mu(X + X', Z + Z')\mu(X', Z')\}.$$

We assume that the typical propagation distance in the Z-direction is L_z, the transverse variation (say, of the initial pulse profile) is L_x, and k_0 is a central wavenumber associated with our source. We obtain the dimensionless form of (3) by introducing the dimensionless variables $X = L_x x$, $Z = L_z z$, $K = k_0 k$ and rewriting the equation as

$$2ik \left(\frac{1}{k_0 L_z} \right) \frac{\partial \psi}{\partial z} + \left(\frac{1}{k_0 L_x} \right)^2 \Delta_x \psi + k^2 \sigma_0 \mu \left(\frac{z L_z}{l}, \frac{x L_x}{l} \right) \psi = -\frac{1}{(k_0 L_z)^2} \frac{\partial^2 \psi}{\partial z^2} \,. \tag{4}$$

We assume now that the medium fluctuates on a relatively fine scale and accordingly introduce the small parameters $\varepsilon_x = l / L_x$ and $\varepsilon_z = l / L_z$. Then (4) takes the form

$$2ik \left(\frac{\varepsilon_z}{k_0 l} \right) \frac{\partial \psi}{\partial z} + \left(\frac{\varepsilon_x}{k_0 l} \right)^2 \Delta_x \psi + k^2 \sigma_0 \mu \left(\frac{z}{\varepsilon_z}, \frac{x}{\varepsilon_x} \right) \psi = -\frac{\varepsilon_z^2}{(k_0 l)^2} \frac{\partial^2 \psi}{\partial z^2} \,, \tag{5}$$

In the parabolic approximation we assume that the right side of (5) is small and can be dropped, leading to

$$2ik \left(\frac{\varepsilon_z}{k_0 l} \right) \frac{\partial \psi}{\partial z} + \left(\frac{\varepsilon_x}{k_0 l} \right)^2 \Delta_x \psi + k^2 \sigma_0 \mu \left(\frac{z}{\varepsilon_z}, \frac{x}{\varepsilon_x} \right) \psi = 0. \tag{6}$$

Let us explain the physical meaning of the small parameters: ε_x measures the overall width of the initial pulse relative to the correlation length l of the random fluctuations – this is

a parameter we may control by choosing the appropriate initial pulse. The parameter ε_z measures the ratio of l to the overall penetration depth – this parameter may be controlled by taking measurements in an appropriate physical location. The third non-dimensional physical parameter $\delta_0 = k_0 l$ can be chosen by taking the appropriate central frequency. We will choose $k_0 l = 1$ which gives the full interaction of the medium with the pulse. The one physical parameter that we can not control but which is given to us by the physics of the problem is σ_0. Then (6) becomes

$$2ik\varepsilon_z \frac{\partial \psi}{\partial z} + \varepsilon_x^2 \Delta_x \psi + k^2 \sigma_0 \mu \left(\frac{z}{\varepsilon_z}, \frac{x}{\varepsilon_x} \right) \psi = 0. \tag{7}$$

We are interested in the paraxial regime when $\varepsilon_z \ll \varepsilon_x$ (recall that the parameters ε_z and ε_x can be chosen by the measurement and probing procedures, respectively). We will consider two ways to approach this regime: first, assume that $\varepsilon_z = \varepsilon_x^2$, and $\varepsilon_x = \sigma_0$, and, further, approximate the "fast" fluctuations in z by a white noise process. This is the Itô-Schrödinger regime [5, 6]. Another possibility is to consider the isotropic regime $\varepsilon_x = \varepsilon_z$, perform the limit $\varepsilon_x = \varepsilon_z \to 0$, and later pass to the narrow beam scaling.

From the asymptotic analysis of (7), we will obtain expressions for the average amplitude $\mathbb{E}(\psi)$ and consequently for the average wavefield $\mathbb{E}(u)$. Such results will characterize the broadening of the pulse and the decay of the amplitude, and can be seen as the three-dimensional analog to the O'Doherty Anstey theory [10, 13]. We will see that the amplitude decays only algebraically and not exponentially in time, due to the signal low/midrange frequency component. Moreover, we will propose an optimal frequency tuning of the source for a given depth. Numerical simulations will be offered to illustrate the results.

The paper is structured as follows: section 2 is devoted to the Itô-Schrödinger regime and section 3 to the isotropic case. Section 4 is concerned with the generalized O'Doherty Anstey theory. The question of deep probing in clutter is addressed in section 5, and the numerical results are proposed in section 6.

2. The Itô-Schrödinger regime

This section is devoted to the Itô-Schrödinger regime where we first assume that $\varepsilon_z = \varepsilon_x^2$. We will compute the average wavefield $\mathbb{E}(u)$ using the mean zero property of stochastic integrals. The choice $\varepsilon_z = \varepsilon_x^2$ gives from (7)

$$\frac{\partial \psi}{\partial z} + \frac{1}{2ik} \Delta_x \psi + \frac{k}{2i\sqrt{\varepsilon_z}} \mu \left(\frac{z}{\varepsilon_z}, \frac{x}{\varepsilon_x} \right) \psi = 0. \tag{8}$$

Let us assume that the smallness of the ratio $\varepsilon_z/\varepsilon_x$ dominates the behavior and the "fast" oscillations in z can be approximated by a white-noise in time, letting $\varepsilon_z \to 0$ at a fixed $\varepsilon_x > 0$. This leads to the Itô-Schrödinger regime when (8) is well approximated by

$$d\psi(x, z, k) = \frac{i}{2k} \Delta_x \psi dz - k^2 R_0 \psi dz + ik\sqrt{R_0} \psi dB_z(\frac{x}{\varepsilon_x}). \tag{9}$$

Here, the stochastic integral is understood in the Itô sense,

$$R_0 = \frac{1}{8} \int_{-\infty}^{\infty} \tilde{R}(s, 0) ds, \qquad \text{and} \qquad \mathbb{E}(dB_z(x) dB_z(x')) = \frac{1}{R_0} \left(\int_{-\infty}^{\infty} \tilde{R}(t, x - x') dt \right) dz.$$

The successive limits $\varepsilon_z \to 0$ first, and then $\varepsilon_x \to 0$, of course, contradict the assumption $\varepsilon_z = \varepsilon_x^2$. However, one can justify this passage rigorously without much difficulty, and accordingly we make the Itô-Schrödinger approximation above as a matter of convenience.

As we have mentioned, another approach to the paraxial regime is starting with the isotropic situation $\varepsilon_z = \varepsilon_x$ and then decreasing the ratio $\varepsilon_z/\varepsilon_x$ to the point where $\varepsilon_z \sim \varepsilon_x^2$. We will also consider this case in section 3

2.1. The average pressure

We compute now the average profile of the pressure u. Consider the "initial" data for the Itô-Schrödinger equation (9) at $z = 0$ given by

$$\psi(x, 0, k) = \alpha(x)\hat{\beta}(k).$$

First, we would like to compute the average $m_1(x, z, k) = \langle \psi(x, z, k) \rangle = \mathbb{E}(\psi(x, z, k))$. Averaging (9) eliminates the martingale part and gives the following equation for m_1:

$$\frac{\partial m_1}{\partial z} = \frac{i}{2k}\Delta_x m_1 - k^2 R_0 m_1.$$

Therefore, the Fourier transform of m_1 in x is

$$\hat{m}_1(\xi, z, k) = e^{-k^2 R_0 z} e^{-i\xi^2 z/(2k)} \hat{\alpha}(\xi)\hat{\beta}(k).$$

Here we define the Fourier transform of a function $f(x)$ as

$$\hat{f}(\xi) = \int e^{-i\xi\cdot x} f(x)dx, \qquad \text{with inverse} \qquad f(x) = \int e^{i\xi\cdot x}\hat{f}(\xi)\frac{d\xi}{(2\pi)^d}.$$

Let us assume that $\hat{\alpha}(\xi) = \alpha_0 e^{-\eta|\xi|^2/2}$ and $\hat{\beta}(k) = \beta_0 e^{-\nu k^2}$ for some real numbers $\eta > 0$, $\beta > 0$, α_0 and β_0. We center the function $\beta(k)$ around $k = 0$ because we are particularly interested in the effect of the low frequencies. Then we have

$$\hat{m}_1(\xi, z, k) = \alpha_0\beta_0 e^{-k^2(R_0 z+\nu)} e^{-\frac{1}{2}(i\frac{z}{k}+\eta)|\xi|^2}.$$

Taking the inverse Fourier transform in ξ gives (recall that d is the dimension of the transverse variable x)

$$m_1(x, z, k) = \alpha_0\beta_0 e^{-k^2(R_0 z+\nu)} \frac{e^{-|x|^2/[2(i\frac{z}{k}+\eta)]}}{(2\pi(i\frac{z}{k}+\eta))^{\frac{d}{2}}}. \tag{10}$$

Let us also assume for simplicity that $\eta = 0$, that, is the initial data is a δ-function in x, and that the transverse dimension is $d = 2$. Then (10) becomes

$$m_1(x, z, k) = \alpha_0\beta_0 e^{-k^2(R_0 z+\nu)} \frac{k e^{-k|x|^2/(2iz)}}{2\pi i z}.$$

We first look at the field on the beam axis.

2.1.1. The field on the beam axis

Going back to (2), we have for $M_1(x,z,T) = \mathbb{E}[u(x,z,T)]$ on the x-axis:

$$M_1(0,z,T) = c_0 k_0 \alpha_0 \beta_0 \int e^{ic_0 k_0 k(L_z z/c_0 - T)} e^{-k^2(R_0 z+\nu)} \frac{k}{iz} \frac{dk}{(2\pi)^2}.$$

We re-center the solution close to the time the front is passing by a point z by taking

$$T = \frac{L_z z}{c_0} + \frac{t}{c_0 k_0}. \tag{11}$$

This gives

$$\begin{aligned} M_1(0,z,t) &= c_0 k_0 \alpha_0 \beta_0 \int e^{-ikt} e^{-k^2(R_0 z+\nu)} \frac{k}{iz} \frac{dk}{(2\pi)^2} \\ &= -\frac{c_0 \alpha_0 \beta_0 k_0}{(4\pi)^{3/2} z} \frac{t}{(R_0 z+\nu)^{3/2}} e^{-t^2/[4(R_0 z+\nu)]}. \end{aligned}$$

Compared to the case where the wave propagates in a homogeneous (i.e when $R_0 = 0$), we thus observe a convolution of the front with a Gaussian function that has variance z in time. This is a defocusing property, and we have broadening of the pulse so that the time-spreading of the pulse at the time it arrives to depth z is of the order $O(\sqrt{z})$. The pulse attains its maximum around the offset time $t_m \sim \sqrt{2R_0 z}$ when it is of the order

$$M_1(0,z,t_m(z)) \sim -\frac{c_0 \alpha_0 \beta_0 k_0}{R_0 z^2}, \quad z \gg 1. \tag{12}$$

We consider now the lateral profile, and we will see that the maximum of the field has the same order as on the x-axis.

2.1.2. The tranverse profile

Let us now look more carefully at the profile in the x variable. We have

$$M_1(x,z,T) = c_0 k_0 \alpha_0 \beta_0 \int e^{ic_0 k_0 k(L_z z/c_0 - T)} e^{-k^2(R_0 z+\nu)} \frac{e^{-|x|^2 k/(2iz)}}{iz} \frac{k dk}{(2\pi)^2},$$

and, after switching to the centered t variable, we obtain

$$\begin{aligned} M_1(x,z,t) &= c_0 k_0 \alpha_0 \beta_0 \int e^{-ikt - k^2(R_0 z+\nu)} \frac{e^{-|x|^2 k/(2iz)}}{iz} \frac{k dk}{(2\pi)^2} \\ &= \frac{c_0 k_0 \alpha_0 \beta_0}{iz} \int e^{-ik(t-|x|^2/(2z)) - k^2(R_0 z+\nu)} \frac{k dk}{(2\pi)^2} \\ &= -\frac{c_0 \alpha_0 \beta_0 k_0}{(4\pi)^{3/2} z} \frac{(t-|x|^2/(2z))}{(R_0 z+\nu)^{3/2}} e^{-(t-|x|^2/(2z))^2/[4(R_0 z+\nu)]}. \end{aligned}$$

For times $t \ll \sqrt{z}$ which, as we have seen, is the lifetime of the pulse at depth z along the propagation axis, and near the axis, for $x \ll \sqrt{2zt}$, the field is approximately uniform in x, and

$$M_1(x,z,t) \approx -\frac{c_0 \alpha_0 \beta_0 k_0}{(4\pi)^{3/2} z} \frac{t}{(R_0 z+\nu)^{3/2}} e^{-t^2/[4(R_0 z+\nu)]}, \quad x \ll \sqrt{2zt}.$$

On the other hand, far away from the axis, with $x \gg \sqrt{2zt}$ we have

$$M_1(x,z,t) \approx \frac{c_0\alpha_0\beta_0 k_0}{(4\pi)^{3/2}2z^2}\frac{x^2}{(R_0 z+\nu)^{3/2}}e^{-x^4/[16z^2(R_0 z+\nu)]}, \quad x \gg \sqrt{2zt}.$$

For $z \gg 1$, this profile attains its maximum around $x_m(z) = R_0^{1/4}(2z)^{3/4}$. At this point we have

$$M_1(x_m(z),z,t) \sim \frac{c_0\alpha_0\beta_0 k_0}{z^2}\frac{R_0^{1/2}z^{3/2}}{(R_0 z)^{3/2}} \sim \frac{c_0\alpha_0\beta_0 k_0}{R_0 z^2}, \quad z \gg 1,$$

which is of the same order as expression (12) for the maximum of the pulse along the propagation axis.

3. The isotropic regime

We consider in this section the isotropic regime where $\varepsilon_x = \varepsilon_z$. We need here a more refined analysis for the computation of $\mathbb{E}(u)$ since the simplification due to the stochastic integral does not hold. We will nevertheless obtain very similar expressions to the Itô-Schrödinger case.

3.1. The wavefield

We consider again the parabolic wave equation (7)

$$2ik\varepsilon_z\frac{\partial\psi}{\partial z} + \varepsilon_x^2\Delta_x\psi + k^2\sigma_0\mu\left(\frac{z}{\varepsilon_z},\frac{x}{\varepsilon_x}\right)\psi = 0 \tag{13}$$

but this time our starting point is the isotropic regime: $\varepsilon_x = \varepsilon_z$, and we drop the subscripts x, z. We also choose $\varepsilon = \sigma_0^2$ – recall, once again, that the parameters ε_x and ε_z are controlled by the choice of the initial data and measurement distance, respectively. Then (13) becomes

$$2ik\varepsilon\frac{\partial\psi}{\partial z} + \varepsilon^2\Delta_x\psi + k^2\sqrt{\varepsilon}\mu\left(\frac{z}{\varepsilon},\frac{x}{\varepsilon}\right)\psi = 0 \tag{14}$$

We also assume that the initial data is ε oscillatory, varies on the scale of the medium fluctuations, and write

$$\psi(z=0,x;k) = \psi_0\left(\frac{x}{\varepsilon};k\right). \tag{15}$$

Let us again re-center the solution close to the front time by taking

$$T = \frac{Lz}{c_0} + \frac{t}{c_0 k_0},$$

with t the new, centered time variable, as in (11). Then we get

$$u(t,x,z) := \frac{1}{2\pi}\int e^{-ikt}\psi\left(z,x;k\right)dk\,,$$

for ψ solving (14)-(15). The medium fluctuations are now assumed to be centered, statistically homogeneous and with strong mixing properties, rather than white noise in z, as in the previous section. In particular, we assume the following form for the medium covariance

$$\check{R}(z,\xi) = e^{-g(\xi)|z|}\hat{R}(\xi)\,, \qquad \check{R}(z,\xi) = \int e^{-i\xi\cdot x} R(z,x)dx\,,$$

for some positive function g. It was shown in [1] that we have the asymptotic characterization

$$\varepsilon^{-d}\hat{\psi}(z,\xi/\varepsilon;k=1) = \left(e^{-zD_\xi/2}\hat{\psi}_0(\xi,k=1) + \hat{Z}(z,\xi)\right)e^{-i|\xi|^2 z/(2\varepsilon)}\,,$$

for Z a centered complex Gaussian field and

$$D_\xi = \frac{1}{2}\int \frac{\hat{R}(p)}{g(p) - i(\xi\cdot p - |p|^2/2)}\frac{dp}{(2\pi)^d}\,.$$

Using the reparameterization $k^2\mu \mapsto \mu, z/|k| \mapsto z, g(\xi)|k| \mapsto g(\xi)$ we obtain

$$\varepsilon^{-d}\hat{\psi}(z,\xi/\varepsilon;k) = \left(e^{-zD_\xi(k)/2}\hat{\psi}_0(\xi,k) + \hat{Z}(z,\xi;k)\right)e^{-i|\xi|^2 z/(2k\varepsilon)}\,, \tag{16}$$

with

$$D_\xi(k) = \frac{k^3}{2}\int \frac{\hat{R}(p)}{kg(p) - i(\xi\cdot p - |p|^2/2)}\frac{dp}{(2\pi)^d}\,.$$

The variance of the process $Z(z,\xi;k)$ is described in [1] in terms of the solution of the radiative transport equation. We will not need its precise form in the present paper, an interested reader is referred to [1] for details.

3.2. Relation to the Wigner transform

In order to understand expression (16) let us restate it in terms of the Wigner transforms [9, 7]. The Wigner transform of two functions f and g is defined as

$$W(x,\xi) = \int e^{i\xi\cdot y} f(x - \frac{\varepsilon y}{2})\bar{g}(x + \frac{\varepsilon y}{2})\frac{dy}{(2\pi)^d},$$

hence

$$\begin{aligned}\int W[f,g](x,\xi)dx &= \int e^{i\xi\cdot y} f(x - \frac{\varepsilon y}{2})\bar{g}(x + \frac{\varepsilon y}{2})\frac{dydx}{(2\pi)^d} = \frac{1}{\varepsilon^d}\int e^{i\xi\cdot(y-x)/\varepsilon} f(x)\bar{g}(y)\frac{dydx}{(2\pi)^d} \\ &= \frac{1}{(2\pi\varepsilon)^d}\hat{f}(\frac{\xi}{\varepsilon})\bar{\hat{g}}(\frac{\xi}{\varepsilon}).\end{aligned}$$

Note that

$$e^{i|\xi|^2 z/(2k\varepsilon)} = \bar{\hat{G}}_\varepsilon(z,\frac{\xi}{\varepsilon};k),$$

where $G_\varepsilon(z,x;k)$ satisfies

$$ik\varepsilon\frac{\partial G_\varepsilon}{\partial z} + \frac{\varepsilon^2}{2}\Delta G_\varepsilon = 0, \quad G_\varepsilon(0,x) = \delta(x),$$

and is given explicitly by

$$G_\varepsilon(z,x) = \frac{1}{\varepsilon^d} G\left(\frac{z}{2k\varepsilon}, \frac{x}{\varepsilon}\right) = \frac{(2k)^{d/2}}{(4\pi\varepsilon i z)^{d/2}} e^{-k|x|^2/(2\varepsilon i z)}.$$

Define now

$$\hat{\zeta}_\varepsilon(z,\xi,k) = \frac{1}{\varepsilon^d}\hat{\psi}(z,\frac{\xi}{\varepsilon},k) e^{i|\xi|^2 z/(2k\varepsilon)},$$

then

$$\hat{\zeta}_\varepsilon(t,\xi;k) = \frac{1}{\varepsilon^d}\hat{\psi}(z,\frac{\xi}{\varepsilon},k)\bar{\hat{G}}_\varepsilon(t,\frac{\xi}{\varepsilon};k) = (2\pi)^d \int W[\psi_\varepsilon, G_\varepsilon](t,\xi,x)dx.$$

Hence, this renormalized wave field can be expressed in terms of the Wigner transform of the full wave function and the Green's function in the homogeneous medium – this essentially corresponds to back-propagation in a homogeneous medium in time-reversal, that is known to produce statistically stable results [12]. In particular, the statistical stability of the Wigner transforms implies the independence of $\hat{\zeta}_\varepsilon(t,\xi;k)$ for different values of ξ or k. This means that the values of the fluctuation process $\hat{Z}(z,\xi,k)$ are independent for different frequencies k.

3.3. The field on the beam axis

In order to relate the above to the near axis field we look at the wave field at the microscopic distances of the order $Z \sim O(\varepsilon^{-1})$ and $X \sim O(\varepsilon^{-1})$. Accordingly, we consider

$$u(t,\varepsilon x,z) = \varepsilon^{-d} \iint \hat{\psi}(z,\xi/\varepsilon;k) e^{-i(kt-\xi\cdot x)} \frac{dkd\xi}{(2\pi)^{d+1}}\,.$$

We shall here in particular assume the tensor product form of the medium correlations

$$g(\xi) \equiv g_0\,,$$

with $g_0 \gg 1$. Then realizations of the random medium can be generated in the tensor product form with the z dependent part being an Ornstein Uhlenbeck process. The situation with g_0 large corresponds to the medium decorrelating rapidly in the depth direction. When $g_0 \gg 1$ we may approximate

$$D_\xi \approx \frac{k^2 R_0}{2g_0}, \quad g_0 \gg 1, \tag{17}$$

which is essentially the Ito-Schrödinger approximation. We find from (16) the representation

$$u(t,\varepsilon x,z) = \int \left(e^{-zD_\xi(k)/2}\hat{\psi}_0(\xi;k) + \hat{Z}(z,\xi;k)\right) e^{-i|\xi|^2 z/(2k\varepsilon)} e^{-i(kt-\xi\cdot x)} \frac{dkd\xi}{(2\pi)^{d+1}}.$$

This can be further transformed as

$$\begin{aligned} u(t,\varepsilon x,z) &= \int \left(e^{-zD_\xi(k)/2}\psi_0(y;k) + Z(z,y;k)\right) \hat{G}_\varepsilon(z,\frac{\xi}{\varepsilon};k) e^{-i(kt-\xi\cdot x)-i\xi\cdot y} \frac{dkd\xi dy}{(2\pi)^{d+1}} \\ &= \varepsilon^d \int \left(e^{-zD_0(k)/2}\psi_0(y;k) + Z(z,y;k)\right) G_\varepsilon(z,\varepsilon x - \varepsilon y;k) e^{-ikt} \frac{dkdy}{2\pi}. \end{aligned}$$

We obtain

$$u(t,\varepsilon x,z)=\int\left(e^{-zD_0(k)/2}\psi_0(y;k)+Z(z,y;k)\right)\frac{(2k\varepsilon)^{d/2}}{(4\pi iz)^{d/2}}e^{-\varepsilon k|x-y|^2/(2iz)}e^{-ikt}\frac{dkdy}{2\pi}.$$

For small $\varepsilon\ll 1$ this becomes

$$u(t,\varepsilon x,z)=\int\left(e^{-zD_0(k)/2}\psi_0(y;k)+Z(z,y;k)\right)\frac{(2k\varepsilon)^{d/2}}{(4\pi iz)^{d/2}}e^{-ikt}\frac{dkdy}{2\pi}.$$

As $\mathbb{E}(Z)=0$, it follows that

$$\begin{aligned}\mathbb{E}(u)(t,\varepsilon x,z) &= \int e^{-zD_0(k)/2}\psi_0(y;k)\frac{(2k\varepsilon)^{d/2}}{(4\pi iz)^{d/2}}e^{-ikt}\frac{dkdy}{2\pi}\\ &= \int e^{-zD_0(k)/2}\hat{\psi}_0(0;k)\frac{(2k\varepsilon)^{d/2}}{(4\pi iz)^{d/2}}e^{-ikt}\frac{dk}{2\pi}.\end{aligned}$$

Moreover, as $Z(z,y;k)$ decorrelates rapidly in k, we believe that we actually have a stronger result, namely $u(t,\varepsilon x,z)$ converges to a deterministic limit, that is, we have

$$u(t,\varepsilon x,z)=\int e^{-zD_0(k)/2}\hat{\psi}_0(0;k)\frac{(2k\varepsilon)^{d/2}}{(4\pi iz)^{d/2}}e^{-ikt}\frac{dk}{2\pi}. \tag{18}$$

This, however, remains an open problem at the moment. Note that the right side of (18) is independent of x, that is, the field becomes uniform near the propagation axis on the microscopic scale $O(\varepsilon)$. We will later analyze its variations on a slightly bigger scale $O(\sqrt{\varepsilon})$ where it becomes non-trivial.

4. Generalized O'Doherty-Anstey Theory

We develop in this section a three-dimensional version of the O'Doherty-Anstey theory [10, 13]. We characterize the spreading and decay of the average wavefield.

4.1. The field on the beam axis

In order to consider the transmitted field along the direction of propagation we use (18) for the average transmitted field on the central axis:

$$v(t,z)=\mathbb{E}(u)(t,0,z)\approx\left(\frac{\varepsilon}{2\pi iz}\right)^{d/2}\int e^{-zD_0(k)/2}\hat{\psi}_0(0;k)k^{d/2}e^{-ikt}\frac{dk}{2\pi}.$$

Let us assume that the fluctuations in the z-direction are fast, in the sense that approximation (17) holds, that is, $D_0(k)=\theta k^2$, with

$$\theta=2R(0)/g_0\,,$$

and the transverse dimension $d=2$. Note that the regime $\theta\ll 1$ essentially corresponds to the Itô-Schrödinger regime, when fluctuations of the random medium in the direction of propagation is much faster than in the transverse direction. This gives

$$v(t,z)=\frac{w(t,z)}{z},$$

with

$$w(t,z) = \frac{\varepsilon}{2\pi i}\int e^{-z\theta k^2/2 - ikt} k\hat{\psi}_0(0;k)\frac{dk}{2\pi}.$$

Note that the function $w(t,z)$ satisfies the diffusion equation,

$$w_z = \frac{\theta}{2} w_{tt},$$

with the propagation distance z playing the role of the time variable, and the local off-set time t playing the role of the spatial variable. The initial condition is

$$w(t,0) = \frac{\varepsilon}{2\pi i}\int e^{-ikt} k\hat{\psi}_0(0;k)\frac{dk}{2\pi} = \frac{\varepsilon}{2\pi}\frac{\partial\tilde{\psi}_0(0;t)}{\partial t}.$$

Here $\tilde{\psi}_0(0;t)$ is the Fourier transform of the incoming pulse $\psi(x,z=0,t)$ in the transverse variable x. This is the three-dimensional analog of the O'Doherty-Anstey (ODA) theory – the pulse spreads as it propagates in the z direction.

In order to discuss some implications of the ODA theory we write this as, with $\xi = k\sqrt{z\theta}$

$$v(t,z) = \frac{\varepsilon}{z\sqrt{z\theta}}\int e^{-\frac{\xi^2}{2} - i\xi t/\sqrt{z\theta}}\tilde{\psi}\left(\frac{\xi}{\sqrt{z\theta}}\right)\frac{d\xi}{(2\pi)^2},$$

with $\tilde{\psi}(k) = -ik\hat{\psi}_0(0;k)$. We define the renormalized local time and propagation distance

$$s = \frac{t}{\sqrt{z\theta}}, z' = z\theta,$$

and introduce the central axis pulse by

$$\bar{v}(s,z') = \frac{v(t,z)}{\theta\varepsilon} = \frac{1}{(z')^{3/2}}\int e^{-\frac{\xi^2}{2} - i\xi s}\tilde{\psi}\left(\frac{\xi}{\sqrt{z'}}\right)\frac{d\xi}{(2\pi)^2}. \tag{19}$$

Let the effective central source trace be

$$\check{\psi}(r) = \frac{1}{2\pi}\int e^{-ir\xi}\tilde{\psi}(\xi)d\xi.$$

We then have

$$\bar{v}(s,z') = \frac{1}{(z')^{3/2}}\int e^{-(s-r)^2/2}\sqrt{z'}\check{\psi}(\sqrt{z'}r)\frac{dr}{(2\pi)^{3/2}},$$

a generalized version of the ODA description of the transmitted pulse. Assume now relatively deep probing, $z' \gg 1$, but with $s = \mathcal{O}(1)$, so that $t = \mathcal{O}(\sqrt{z'}) \gg 1$, then we have

$$\bar{v}(s;z') \;=\; \frac{c_\psi}{(z')^2}\frac{se^{-s^2/2}}{\sqrt{2\pi}}, z' \gg 1, \quad c_\psi = \int \psi_0(x,0)dx.$$

Thus, in this frame, we observe derivative of a Gaussian pulse, of unit width, and whose amplitude decays as z^{-2}. Note that in original coordinates the width of the Gaussian scales as $\sqrt{z}$ in the temporal coordinate t.

4.2. The field near the beam axis

We now look at the wave field on a broader beam, on a lateral scale so that the wave field has a non-trivial lateral structure. We thus look at the wave field at the microscopic distances of the order $Z \sim O(\varepsilon^{-1})$ and $X \sim O(\varepsilon^{-1/2})$. Accordingly, using (18) and (19) we consider

$$\mathbb{E}(u)(t, \sqrt{\varepsilon}x, z) = \int \left(e^{-zD_0(k)/2}\psi_0(y;k)\right) \frac{(2k\varepsilon)^{d/2}}{(4\pi iz)^{d/2}} e^{-k|x-\sqrt{\varepsilon}y|^2/(2iz)} e^{-ikt} \frac{dkdy}{2\pi}. \quad (20)$$

Letting $\varepsilon \to 0$ this becomes, with $d = 2$,

$$\begin{aligned} \mathbb{E}(u)(t, \sqrt{\varepsilon}x, z) &\approx \int \left(e^{-zD_0(k)/2}\psi_0(y;k)\right) \frac{(2k\varepsilon)}{(4\pi iz)} e^{-k|x|^2/(2iz)} e^{-ikt} \frac{dkdy}{2\pi} \\ &= \int \left(e^{-zD_0(k)/2}\hat{\psi}_0(0;k)\right) \frac{(2k\varepsilon)}{(4\pi iz)} e^{-ik(t-|x|^2/(2z))} \frac{dk}{2\pi} \\ &= v(t - \frac{|x|^2}{2z}, z), \end{aligned}$$

with $v(t, z)$ given by the right side of (19). Therefore, the transverse spatial profile around the beam axis is a simple transformation of the field on the axis, as we have observed in the Itô-Schrödinger regime.

4.3. Broader beams

Let us now assume the initial data is of the form $\psi_0(y) = \varepsilon^{d/2}\psi_0(\sqrt{\varepsilon}y)$, that is, the pulse is broad in the transverse direction. The latter assumption, formally, takes us outside the regime of validity of (16), but let us disregard this fact that, we believe, is technical in nature. Then we obtain, instead of (20), with $d = 2$:

$$\begin{aligned} \mathbb{E}(u)(t, \sqrt{\varepsilon}x, z) &= \varepsilon \int \left(e^{-zD_0(k)/2}\psi_0(\sqrt{\varepsilon}y;k)\right) \frac{(2k\varepsilon)}{(4\pi iz)} e^{-k|x-\sqrt{\varepsilon}y|^2/(2iz)} e^{-ikt} \frac{dkdy}{2\pi} \\ &= \varepsilon \int e^{-zD_0(k)/2}\psi_0(y;k) \frac{(2k)}{(4\pi iz)} e^{-k|x-y|^2/(2iz)} e^{-ikt} \frac{dkdy}{2\pi}. \end{aligned}$$

Now, the field around the axis is modified in a non-trivial way that agrees with the ODA picture. Let us define

$$p(z, x, k) = \int e^{-zD_0(k)/2}\psi_0(y;k) \frac{(2k)}{(4\pi iz)} e^{-k|x-y|^2/(2iz)} \frac{dy}{2\pi}.$$

This function satisfies the homogenized Schrödinger equation

$$ip_z + \frac{k}{2}\Delta p + \frac{iD_0(k)}{2}p = 0, \quad p(0, x, k) = \psi_0(x;k),$$

and

$$\mathbb{E}(u)(t, \sqrt{\varepsilon}x, z) = \varepsilon \int p(z, x, k) e^{-ikt} \frac{dk}{2\pi}.$$

This is essentially the homogenization regime.

5. Deep probing through clutter

We investigate here the frequency content of the wavefield and the influence of low frequencies on its amplitude.

5.1. Probing a given depth

Assume that we want to probe a target at a particular depth z, or transmit a pulse through a slab of width z. It is then clear from (20) that the optimal source pulse that has optimal transmission and concentration properties should satisfy the scaling:

$$\check{\psi}(s) \propto f\left(\frac{s}{\sqrt{z\theta}}\right) .$$

We assume here that there is a limit on the source amplitude. Thus, as we probe deeper through the clutter the frequency content of the source is scaled down. The result (20) tells exactly how to implement this scaling. It is also clear that what is important from the point of view of probing is this frequency tuning rather than the exact shape f of the source.

Finally, we remark that if we choose

$$\psi(z=0,\mathbf{0};k) = \sqrt{z\theta}\psi_0\left(\mathbf{0};\sqrt{z\theta}k\right) , \tag{21}$$

corresponding to a fixed amplitude constraint of the time source trace, then indeed the optimal depth tuned signal decays as $\mathcal{O}(z^{-3/2})$ with respect to depth in amplitude, while the support scales as $\mathcal{O}(\sqrt{z})$.

5.2. Probing with a strict low frequency cutoff

We have indeed that $\tilde{\psi}(0) = 0$ so that to realize the optimal $z^{-3/2}$ amplitude decay with respect to depth we have to tune the source frequency contents as discussed above. One may indeed have constraint on the low frequency contents of the probing pulse and this will affect the probing range. To analyze this aspect we now shift a focus in that we assume a given initial pulse with a low frequency cutoff and analyze the pulse as it propagates deep into the medium. Specifically, we assume here a source trace of the form (for $k > 0$):

$$\psi_0(\mathbf{0};k) = \mathbf{I}_{k>\delta}(k)\alpha|k-\delta|^p h(k) ,$$

for $h(\delta) = 1$ and h a smooth function of rapid decay at infinity, p a positive integer and α a fixed positive parameter. We shall first assume that δ is strictly positive.

We write the transmitted pulse in (19) in the form:

$$\bar{v}(N;\sqrt{z\theta}) = \frac{4\pi}{(z\theta)^{3/2}}\Re\left[\int_0^\infty e^{-\frac{\xi^2}{2}-i\xi N}\tilde{\psi}\left(\frac{\xi}{\sqrt{z\theta}}\right)d\xi\right] ,$$

with now

$$\tilde{\psi}\left(\xi\right) = (2\pi)\psi_0(\mathbf{0};\xi)|\xi| .$$

We first note that at the arrival time of the pulse, corresponding to $N = 0$ we have:

$$\bar{v}(0;\sqrt{z\theta}) = \mathcal{O}\left(z^{-2}e^{-\frac{\delta^2 z\theta}{2}}\right) .$$

Therefore, we see that at the depth scaling $z = \mathcal{O}((\theta\delta^2)^{-1})$ there is a transition from power law to exponential decay.

We are now interested in the pulse tail asymptotics corresponding to depths $N \gg 1$. Using integration by parts we find:

$$\bar{v}(N; \sqrt{z\theta}) \overset{N\to\infty}{=} \frac{4\pi\alpha\delta p! e^{\frac{-\delta^2 z\theta}{2}}}{(z\theta)^{(3+p)/2} N^{p+1}} \begin{cases} \cos(N\delta\sqrt{z\theta})(-1)^{\frac{p+1}{2}} & p \text{ odd} \\ \sin(N\delta\sqrt{z\theta})(-1)^{\frac{p-1}{2}} & p \text{ else} \end{cases} .$$

Again, we see that there is a transition zone in between power law decay and exponential damping with respect to depth for $z = \mathcal{O}((\theta\delta^2)^{-1})$. Moreover, there is a relation in between smoothness of low frequency cutoff and pulse tail decay. The smoother the cutoff, the less low frequencies contains the pulse, and the faster is the power law decay (in n) for the tails. Note also the oscillation in the tails, at a frequency corresponding to the low frequency cutoff.

5.3. Probing with a zero frequency cutoff

We consider here the case with $\delta = 0$, corresponding to the initial data with vanishing (smoothly) only at zero frequency. We then have

$$\bar{v}(N; \sqrt{z\theta}) \overset{N\to\infty}{=} \frac{4\pi\alpha(p+1)!}{(z\theta)^{(4+p)/2} N^{p+2}} \begin{cases} \cos(N\sqrt{z\theta})(-1)^{\frac{p+2}{2}} & p \text{ even} \\ \sin(N\sqrt{z\theta})(-1)^{\frac{p-1}{2}} & p \text{ else} \end{cases} .$$

Observe that in this case there is no transition zone to exponential decay, however, the power law decay with respect to depth is more rapid. A smooth low frequency cutoff, corresponding to large p, gives a relatively rapid power law decay with respect to depth. Note also that, the power law decay of the pulse tails is somewhat more rapid than in the case with strict low frequency cutoff.

6. Numerical results

We present in this section numerical simulations illustrating the theory. We set $d = 1$, so that waves propagate in two dimensions and we solve the Schrödinger equation in one dimension. We focus first on the wavefunction ψ and in a second time on the pressure u obtained after integration over the frequency variable. We describe below the numerical method and the parameters setting.

6.1. Numerical scheme

We solve the one-dimensional Itô-Schrödinger equation (9), recast in Stratonovich form as

$$d\psi(z, x; k) = \frac{i}{2k}\Delta\,\psi\,dz + \frac{ik\sigma_0}{2}\psi \circ dW_z\,(x)\,, \qquad z > 0, \quad x \in \mathbb{R}, \tag{22}$$

where we recall that k is the (rescaled) wavenumber and σ_0 measures the amplitude of the random fluctuations. The Wiener process W_z is obtained by the classical formula [4]

$$W_z(x) = \sum_{n\geq 1} \beta_n(z)(\Phi e_n)(x),$$

where $(\beta_n(z))_{n\geq 1}$ is a sequence of independent standard Brownian motions, $(e_n)_{n\geq 1}$ is a basis of $L^2(\mathbb{R})$, and Φ is an integral operator defined by

$$(\Phi e_n)(x) = \int_{\mathbb{R}} c(x-y)e_n(y)dy, \qquad c(x) = \frac{1}{(2\pi\sigma_c^2)^{\frac{1}{4}}} e^{-\frac{x^2}{4\sigma_c^2}}.$$

The function c was chosen so that $\|c\|_{L^2} = 1$. The correlation function of dW_z then reads

$$\mathbb{E}(dW_z(x)\, dW_{z'}(y)) = \min(z, z')\, R(x-y), \qquad R(x) = \int_{\mathbb{R}} c(x-y)c(y)dy.$$

The correlation length ε_x and the absorption term R_0 of (9) are given by

$$\varepsilon_x = \int_{\mathbb{R}} R(x)dx = \|c\|_{L^1}^2 = 2\sqrt{2\pi}\sigma_c, \qquad R_0 = \frac{\sigma_0^2}{8}\|c\|_{L^2}^2 = \frac{\sigma_0^2}{8}.$$

The initial condition $\alpha(x)$ is a Gaussian with standard deviation σ_I:

$$\alpha(x) = \frac{1}{(2\pi\sigma_I^2)^{\frac{1}{2}}} e^{-\frac{x^2}{2\sigma_I^2}}. \tag{23}$$

Equation (22) is discretized on the interval $[-L, L]$ using a grid of $N+1$ points and appropriate absorbing boundary conditions in order to simulate the propagation over the whole space. It is solved using a classical Strang splitting scheme as follows: for a time (z actually) stepsize $h > 0$, let

$$\begin{aligned} \mathcal{A} &= \frac{i}{2k}\Delta \\ \mathcal{B}(z) &= \frac{ik\sigma_0}{2}(W_{z+\frac{h}{2}}(x) - W_z(x)). \end{aligned}$$

The semi-discrete scheme then reads

$$\psi_m = e^{\mathcal{B}(z_{m-1}+\frac{h}{2})} e^{h\mathcal{A}} e^{\mathcal{B}(z_{m-1})} \psi_{m-1}, \qquad m = 1, 2, \cdots, \qquad \psi_0(x) = \alpha(x),$$

where $\psi_m(x)$ is an approximation of $\psi(z_m, x)$ at $z_m = mh$. Terms involving $e^{h\mathcal{A}}$ are calculated using fast Fourier transforms on $[-L, L]$ and the method of [8] to incorporate absorbing boundary conditions. The basis of $L^2(-L, L)$ for the construction of the random potential is chosen as $e_n(x) = \frac{1}{\sqrt{\Delta x}} \mathbb{1}_{[-L+n\Delta x, -L+(n+1)\Delta x]}(x)$, $n = 0, \cdots, N-1$, with $\Delta x = 2L/N$. In the simulations, we set $N = 400$, $h = 0.01$, $\sigma_I = 1$ and $L = 10\sigma_I$.

6.2. Average wavefunction

We start by comparing the average wavefunction with the theoretical prediction for different fluctuations strengths. The wavenumber k is set to $k = 1$. We choose σ_0 so that $R_0 = 1$ and $R_0 = 0.25$. The parameter σ_c is chosen such that the correlation length ε_x is equal to σ_I, i.e. $\varepsilon_x = \sigma_I = 1$. Results are depicted in figure 1. We represent the (empirical) average of the wavefunction $\mathbb{E}(\psi)$ on the axis $x = 0$ as a function of the depth z, computed for $N_r = 1000, 100$ and 10 realizations of the random medium. Both the real part and the

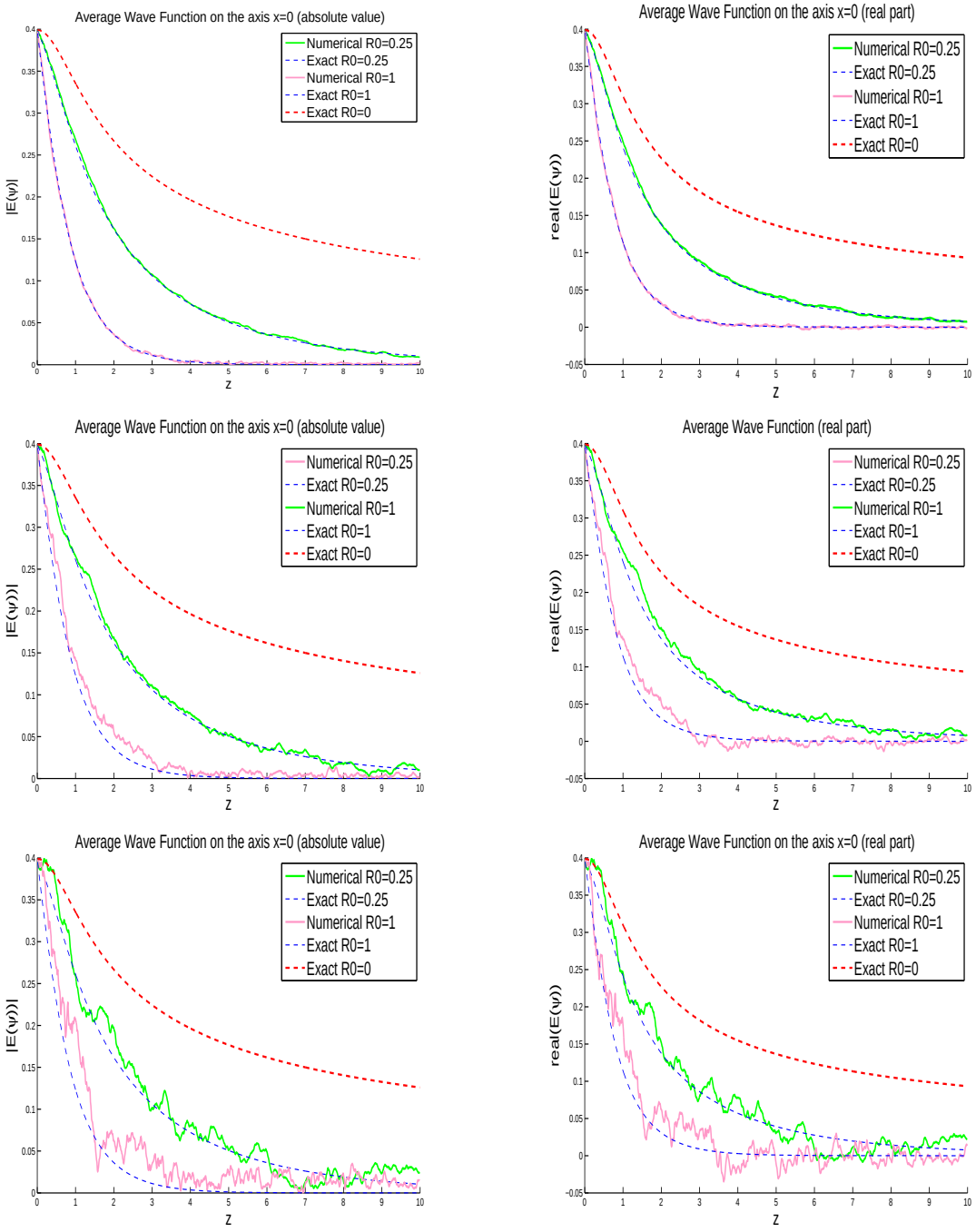

Figure 1: Average wave function on the axis $x = 0$ as a function of z, for $N_r = 1000, 100, 10$, top to bottom, and $R_0 = 0, 0.25, 1$. Left: absolute value, right: real part. Statistical instabilities are observed when $N_r = 10$, while we have an almost perfect match when averaging is strong enough with $N_r = 1000$.

absolute value are shown since they may exhibit different behaviors in some situations as we will see below.

It is clear from the simulations that the theory is matched almost perfectly when $N_r = 1000$. When N_r decreases to 100 and 10, randoms oscillations appear since averaging is not strong enough. As expected, the decay is faster when $R_0 = 1$ than when $R_0 = 0.25$.

Note that the behavior of $\mathbb{E}(\psi)$ is independent of the the correlation length ε_x since the absorption term R_0 only depends on σ_0 and not on σ_c. Such a property holds for averages, but not for single realizations as shown in figure 2 for $R_0 = 0.25$. In the top figures, $\varepsilon_x = \sigma_I = 1$, while in the bottom figures, we have $\varepsilon_x = 10\sigma_I = 10$, so that the correlation length is much larger than the typical support of the initial condition. The influence of the ratio $\frac{\sigma_I}{\varepsilon_x}$ is mostly seen on the absolute value of ψ: while the real part (or of course the imaginary part not shown here) exhibits random fluctuations, roughly around the average, the absolute value is stable and is very close the solution obtained in a homogeneous medium with $R_0 = 0$. This can be explained by the following observation: when $\frac{\sigma_I}{\varepsilon_x} \ll 1$ and z is small enough, then the potential term in the Schrödinger equation $\psi(x) \circ dW_z(x)$ is roughly equal to $\psi(x) \circ dW_z(0)$ since the wavefunction is localized around 0 compared to the random potential. As a consequence, randomness is mostly seen in a time dependent phasis, independent of x, that can be factored out. The absolute value of the wavefunction is then close to the one in a homogeneous medium. The absolute values of ψ for $\varepsilon_x = 1$ and $\varepsilon_x = 10$ are depicted in figure 3 as functions of (x, z). Note the very different behaviors.

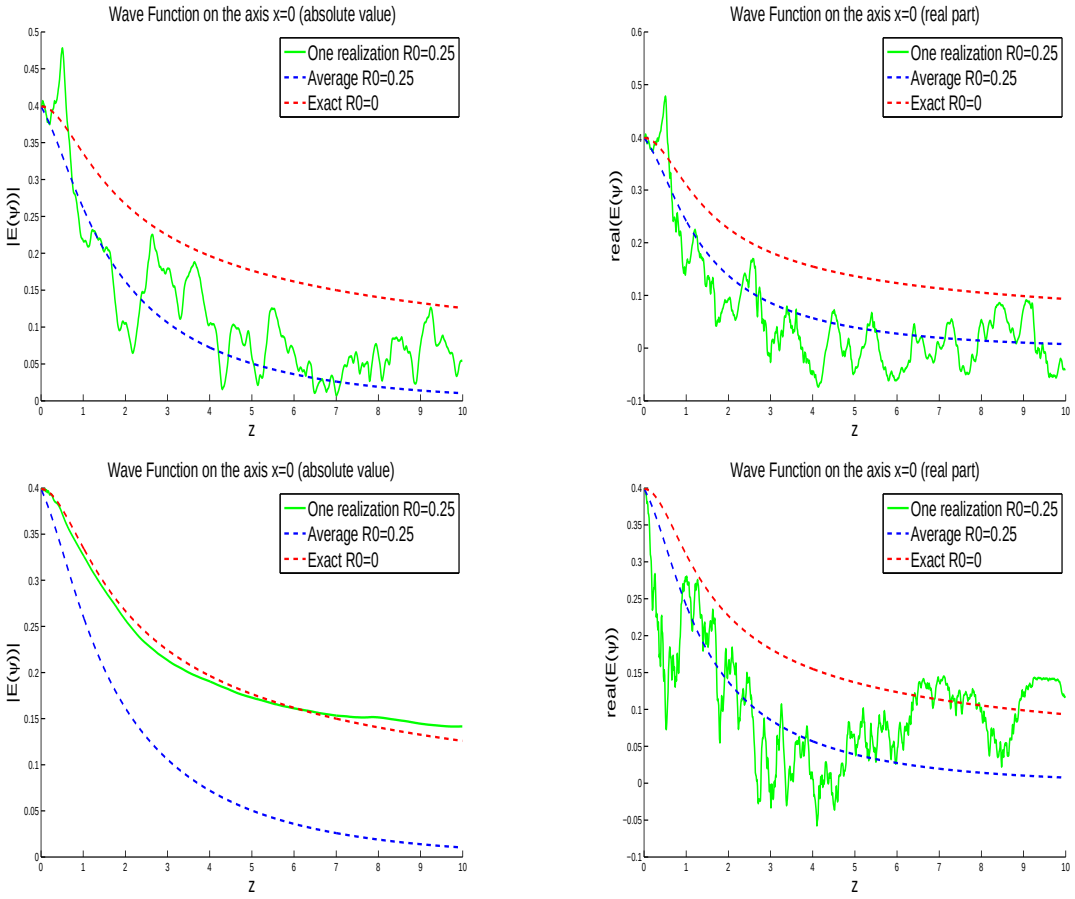

Figure 2: One realization wave function on the axis $x = 0$ as a function of z, for $\varepsilon_x = \sigma_I = 1$ (top) and $\varepsilon_x = 10\sigma_I = 10$ (bottom), with $R_0 = 0.25$. Left: absolute value, right: real part. When $\varepsilon_x = 10\sigma_I = 10$, the absolute value is close to the homogeneous solution, while the real part is random. This is due to the fact that when $\varepsilon_x = 10\sigma_I = 10$ and z is not too large, the randomness is is concentrated in a random phase independent of x factored out when taking absolute value.

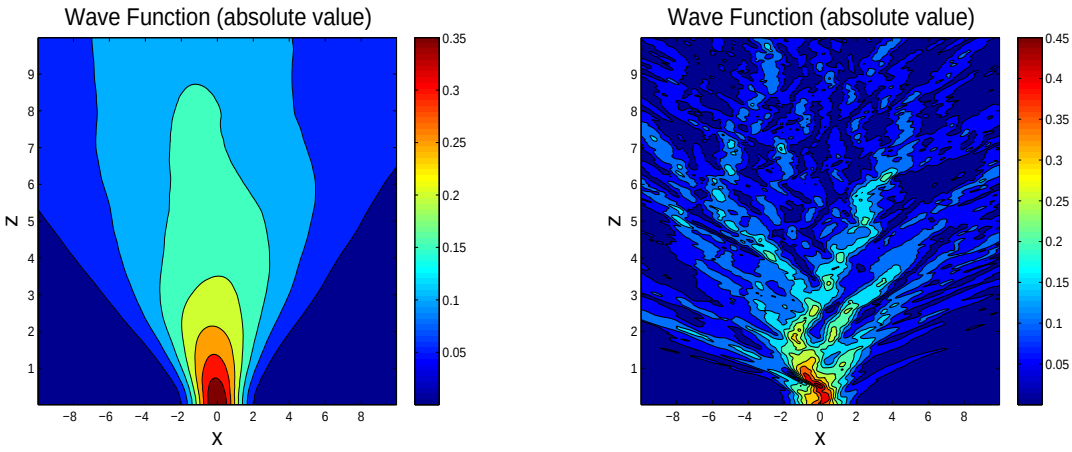

Figure 3: $|\psi(z,x)|$ for one realization for $\varepsilon_x = 10\sigma_I = 10$ (left) and $\varepsilon_x = \sigma_I = 1$ (right), with $R_0 = 0.25$. For the same reasons as in figure 2, $|\psi(z,x)|$ on the left is close to the homogeneous solution, while it is random on the right.

6.3. Dependence of the wavefunction on the frequency

We investigate here the dependence on the frequency. We plot $\mathbb{E}(\psi)$ for $k = 1/2, 1$ and $k = 3$ in figure 4. As expected, the lower the frequency is, the closer the wavefunction to a solution in a homogeneous medium is: when $k = 3$, homogeneous and inhomogeneous solutions are very different (solid and dotted lines), but as k becomes smaller, solutions get closer to each other.

Besides, as explained in section 3, the wavefunctions for different k are expected to decorrelate in a suitable regime. We explore this fact in figure 5 for $R_0 = 0.25$ where we plot the correlation coefficient

$$\begin{aligned} r(k,p,z) &= \frac{|C(z,k,p)|}{(C(z,k,k))^{\frac{1}{2}}(C(z,p,p))^{\frac{1}{2}}}, \\ C(z,k,p) &= \mathbb{E}\left(\psi(z,0;k)\psi^*(z,0;p)\right) - \mathbb{E}(\psi(z,0;k))\mathbb{E}(\psi^*(z,0;p)). \end{aligned}$$

On the axis of propagation $x = 0$, we observe at a depth $z = 1$ (left figure), that the correlation is still very strong between the frequencies. The corresponding modulus of the average wavefunction for $z = 1$ at $x = 0$ is roughly half of the initial value. At $z = 5$, decorrelation can be observed compared to the case $z = 1$, but now the wavefunction is about one tenth of the inital value. At $z = 10$, frequencies are very decorrelated, and the wavefunction has a magnitude divided by a factor 50 compared to the initial value. Thus, as expected, the decorrelation of the wavefunction for different frequencies indeed takes place. But it seems it is a property that is hard to exploit in practice when probing a clutter since the depth at which such decorrelation occurs is too large for the signal to be large enough compared to the statistical instabilities.

6.4. Deep probing through clutter

We verify two facts in this section: (i) that initial conditions of section 5 satisfying the scaling (21) $\psi(z=0,\mathbf{0};k) = \sqrt{z\theta}\psi_0(\mathbf{0};\sqrt{z\theta}k)$ (here in the Itô-Schrödinger regime we have $\theta = R_0$) indeed offer (nearly) optimal pulse transmission; and (ii) that a strict low frequency

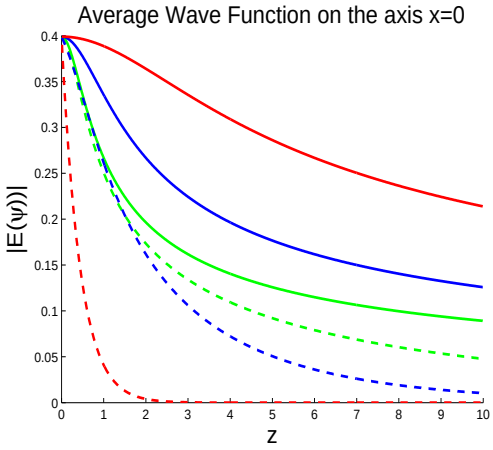

Figure 4: Dependence of $|\mathbb{E}(\psi(z,x))|$ on the wavenumber k. Dotted lines correspond to $R_0 = 0.25$ and $k = 1/2, 1, 3$ (green, blue, red), while solid lines to $R_0 = 0$ (homogeneous solution) and $k = 1/2, 1, 3$. The lower the frequency is, the closer the wavefunction to a solution in a homogeneous medium is.

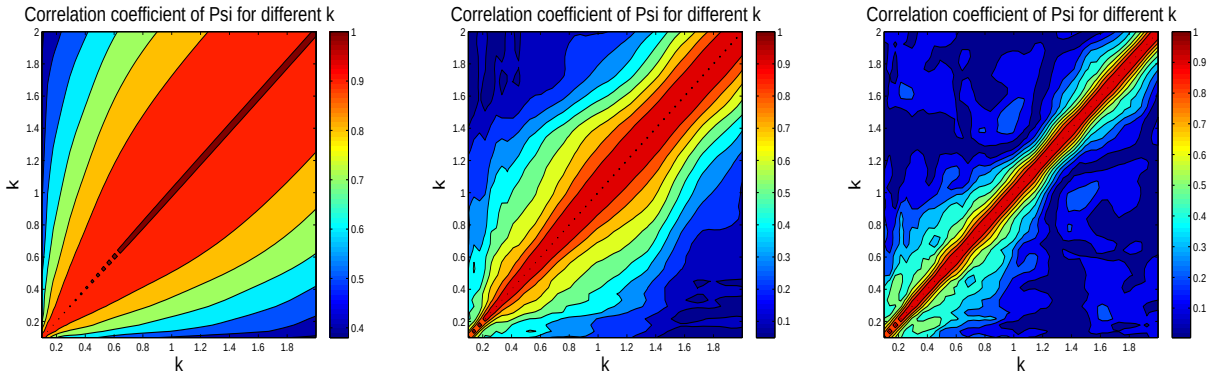

Figure 5: Decorrelation of the wavefunction (on the axis $x = 0$) for different frequencies, for $z = 1$ (left), $z = 5$ (middle), $z = 10$ (right). The modulus of the average wavefunction for $z = 1$ at $x = 0$ is roughly half of the initial value, at $z = 5$ it is one tenth of the inital value, at $z = 10$, it is divided by a factor 50 compared to the initial value. Decorrelation is thus observed but a distance where the wavefunction has strongly decreased.

cutoff yields a wavefront with lower amplitude but with slower tail decay as shown in section 5. For this we look at the values of the average wavefield on the $x = 0$ axis around the front time, given by

$$u_F(t,z) = \frac{1}{2\pi}\int e^{-ikt}\mathbb{E}(\psi)(z, x=0; k)dk$$

with initial conditions at $z = 0$:

$$\psi(z=0,x;k) = \alpha(x)\beta_j(k), \qquad \beta_1(k) = \frac{1}{\sigma_k}e^{-\frac{k^2}{\sigma_k^2}}, \quad \beta_2(k) = \frac{1}{\eta\omega_c + i(k-\omega_c)} + \frac{1}{\eta\omega_c + i(k+\omega_c)}.$$

Above, α is defined in (23), σ_k, η and ω_c are positive parameters. The second frequency profile β_2 is obtained by Fourier transform of the pulse

$$\beta_2(t) = \mathbf{I}_{t>0}(t)2e^{-\eta\omega_c t}\cos\omega_c t,$$

where ω_c is the central frequency and η an absorption parameter. The functions β_j are chosen such that the initial wavefield on the beam axis $u_0 := u(t = 0, x = 0, z = 0) = \frac{1}{2\pi}\int \alpha(0)\beta_j(k)dk$ is independent of σ_k and ω_c, which allows for a fair comparison of the transmission profile. The correlation length ε_x and σ_I are set to one.

In figure 6, left, we consider the frequency profile β_1 and represent the ratio u_F/u_0 at the wavefront time $t = 0$ as a function of σ_k for $R_0 = 1, 1/4, 1/16$ for $z = 5$. It is clearly observed that (i) the smaller the R_0, the better the transmission and (ii) there exist optimal σ_k. These optimal values naturally depends on the exact form of the initial condition. Nevertheless, the theory of section 5 tells us that the choice $\sigma_k = 1/\sqrt{zR_0}$, independent of the initial condition, should yield nearly optimal results. This is confirmed in the left figure, where the dots and straight lines correspond to $\sigma_k = 1/\sqrt{zR_0}$.

In the right figure, we plot u_F/u_0 at $t = 0$, $z = 5$ as a function of σ_k for $R_0 = 1/16$ and three realizations of the random medium. The average value is represented in a solid line. We observe that u_F/u_0 depends on the realization, and that the optimal scaling $\sigma_k = 1/\sqrt{zR_0}$ does not hold any longer. Simulations performed in a two dimensional transverse plane (instead of a one dimensional here) might yield more stable results as lateral diversity should introduce some averaging. Stabilizing the transmission profile is the object of a future work.

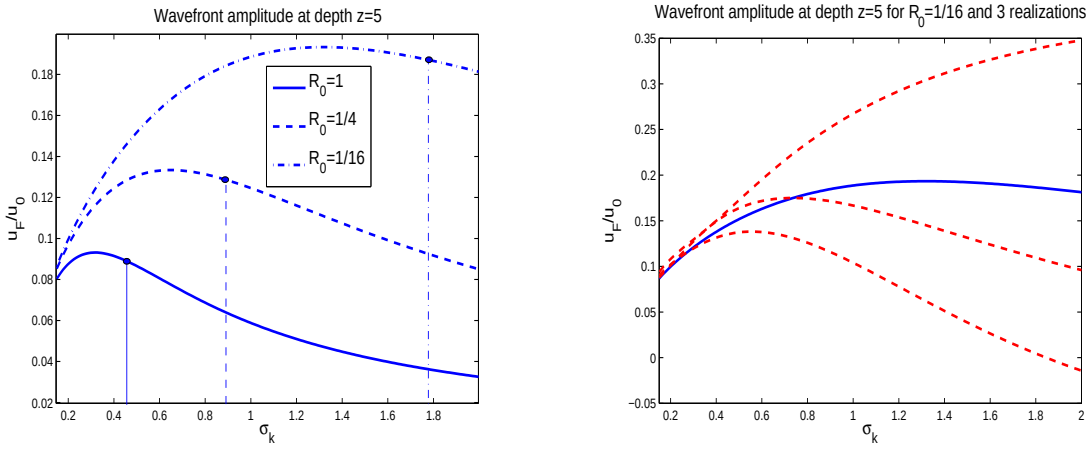

Figure 6: Left: average wavefront amplitude at the front time $t = 0$ as a function of σ_k for $R_0 = 1, 1/4, 1/16$, $z = 5$, $\sigma_I = \varepsilon_x = 1$ and the profile β_1. The vertical lines correspond to the optimal scaling $\sigma_k = 1/\sqrt{zR_0}$. Note the good match with the theory. Right: wavefront amplitude at $t = 0$ for three realizations (dash lines) and average wavefront (solid line) for $R_0 = 1/16$, $z = 5$ and $\sigma_I = \varepsilon_x = 1$. Statistical instabilities modify the value of the optimal scaling.

We confirm in figure 7 the near optimal scaling in $1/\sqrt{zR_0}$ with the second frequency profile β_2 for a different penetration depth. We plot u_F/u_0 at $t = 0$ and $z = 2.5$ for $R_0 = 1, 1/4, 1/16$ as a function of ω_c. The absorption η is set to 0.5 for the simulations involving β_2. In the left figure, the dots and straight lines correspond to $\omega_c = 1/\sqrt{zR_0}$. On the right figure, we represent u_F/u_0 for the three different realizations and observe as before some statistical instabilities.

In figure 8, we investigate the effects of a low frequency cutoff as in section 5. We consider an initial condition with weak low frequency content of the form

$$\psi(z = 0, x; k) = \alpha(x)\beta_2(k)\mathbf{I}_{k>\delta}(k)$$

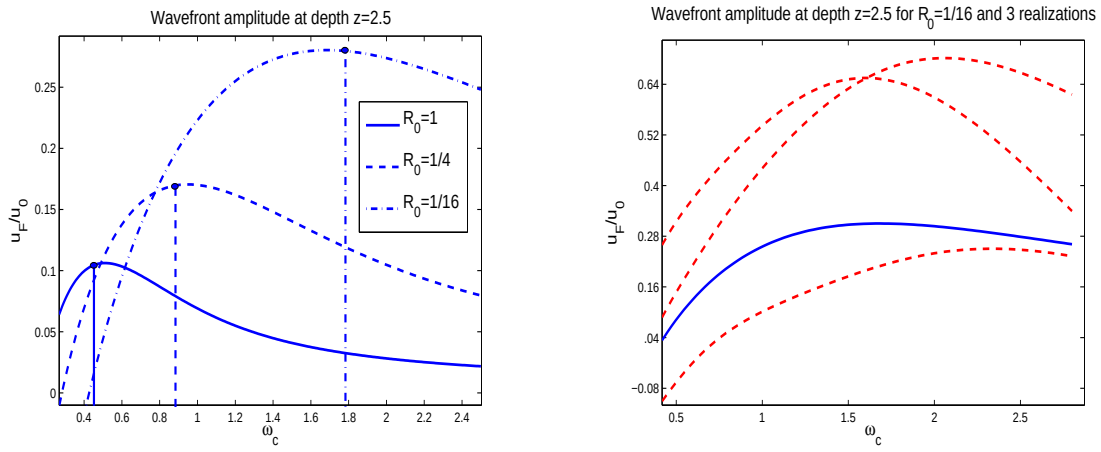

Figure 7: Left: average wavefront amplitude at the front time $t = 0$ as a function of ω_c for $R_0 = 1, 1/4, 1/16$, $z = 2.5$, $\sigma_I = \varepsilon_x = 1$ and the profile β_2. The vertical lines correspond to the optimal scaling $\sigma_k = 1/\sqrt{zR_0}$. Right: wavefront amplitude for three realizations (dash lines) and average wavefront (solid line) for $R_0 = 1/16$, $z = 2.5$ and $\sigma_I = \varepsilon_x = 1$.

for different values of δ. In the left panel of the figure, we set the optimal scaling $\omega_c = 1/\sqrt{zR_0}$ and represent u_F/u_0 at the front time $t = 0$ and $R_0 = 1/16$ as a function of z for several δ. It it clearly seen that low frequencies have a major influence on the amplitude of the wavefront, and that damping them leads to a serious decay of the amplitude.

On the right panel of figure 8, we represent u_F/u_0 at depth $z = 2.5$ as a function of t in order to observe the tail behavior. We set $\omega_c = 1/\sqrt{zR_0}$ and $R_0 = 1/16$. As observed before, the case without cut-off $\delta = 0$ leads to a greater amplitude than when $\delta > 0$. As shown in section 5, this absence of cutoff leads to a faster decay of the tail, which is confirmed in the simulations.

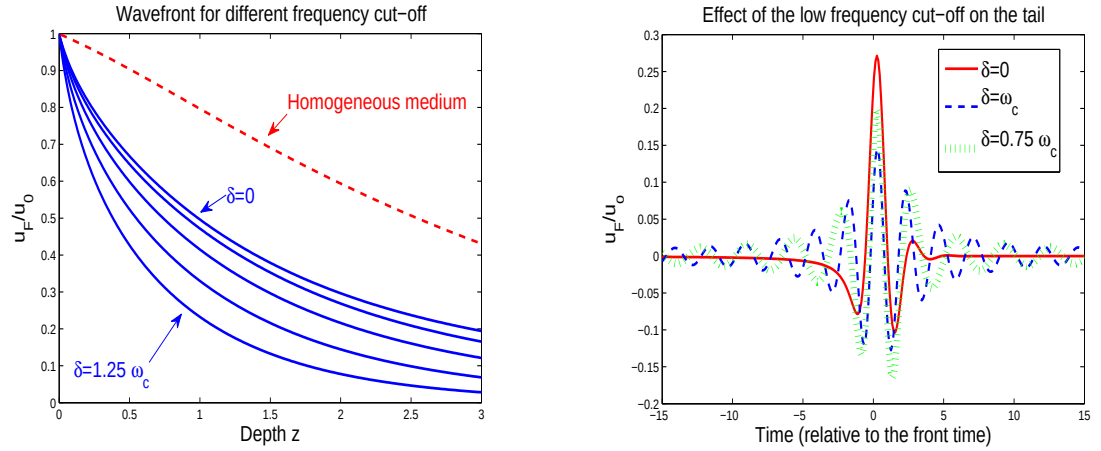

Figure 8: Left: average wavefront amplitude at the front time $t = 0$ as a function of z for $R_0 = 1/16$, $\sigma_I = \varepsilon_x = 1$. The dash line corresponds to the homogeneous case and shows the optimal decay. The solid lines corresponds to, from up to down: $\delta = 0, 0.5\omega_c, 0.75\omega_c, \omega_c, 1.25\omega_c$. The amplitude decreases at the cutoff increases. Right: average wavefront amplitude at $z = 2.5$ as a function of t for $R_0 = 1/16$, $\sigma_I = \varepsilon_x = 1$ and different values of δ. Here again, the amplitude is larger for a small cutoff. Note nevertheless the faster tail decay when δ is small.

In figure 9, we represent for $\delta = 0$ the ratio u_F/u_0 at depth $z = 2.5$ as a function of t as well as the initial profile $\beta_2(t)$ (shifted appropriately) and two realizations of the random medium. The absorption η is lowered to 0.2 in order to have a better look at the oscillations. As expected, we observe some statistical instabilities, but nevertheless the qualitative behavior of the random wavefront is globally similar to the average wavefront.

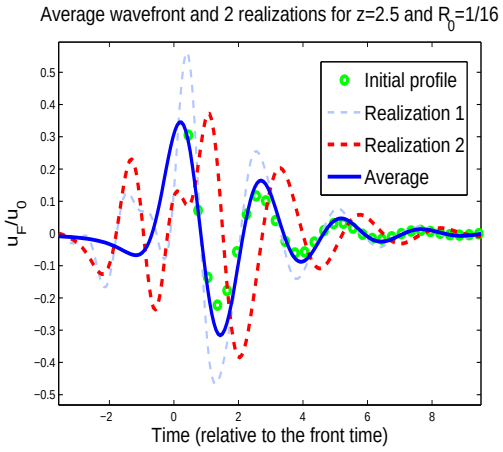

Figure 9: Average wavefront amplitude (solid line) at $z = 2.5$ as a function of t for $R_0 = 1/16$, $\sigma_I = \varepsilon_x = 1$, $\delta = 0$ and 2 realizations (dash lines). The inital profile $\beta_2(t)$ (shifted appropriately) is represented by the circles. The absorption η is equal to 0.2. The qualitative behavior of the random wavefront is similar to the average wavefront.

7. Conclusion

We have developed a three-dimensional generalization of the O'Doherty-Anstey theory. We assumed that the parabolic approximation held and characterized the average wavefield in various asymptotic regimes depending on the medium fluctuations and the measurement setting. As in the one-dimensional case, we showed that the pulse undergoes some spreading as it propagates. We moreover obtained that, thanks to its low frequency component, the average front amplitude decays only algebraically and not exponentially in time. This fact was confirmed by numerical simulations, where signals with low frequency content exhibit a larger amplitude than signals with damped low frequencies. We also characterized and numerically validated the optimal frequency tuning to maximize the transmission of the pulse at a given depth.

The main limitation of this work pertains to statistical instabilities. The presented theory holds only for the average wavefield. While some averaging is expected due to frequency decorrelation as explained in section 3, numerical results show that such effect seems to be taking place at a somewhat large depth where the front has a small amplitude, at least in a two-dimensional configuration. This averaging property might therefore be difficult to exploit in practice. A deeper analysis of the front stabilization will be the object of future research.

References

[1] G. Bal, T. Komorowski, and L. Ryzhik, Asymptotics of the phase of the solutions of the random schrödinger equation, ARMA, (2011), pp. 13–64.

[2] E. H. Bleszynski, M. C. Bleszynski, T. Jaroszewicz and R. Albanese, Imaging with Trains of Wide-band Infra-red Pulses, IEEE Trans. on Ant. and Prop., 6, 1, 2009.

[3] N. A. Cartwright and K. E. Oughstun, Uniform asymptotic applied to ultrawideband pulse propagation, Siam Review **49** (2007) 628–648.

[4] G. Da Prato and J. Zabczyk, Stochastic equations in infinite dimensions, vol. 44 of Encyclopedia of Mathematics and its Applications, Cambridge University Press, Cambridge, 1992.

[5] D. A. Dawson and G. C. Papanicolaou, A random wave process, Appl. Math. Optim., 12 (1984), pp. 97–114.

[6] J. Garnier and K. Sølna, Coupled paraxial wave equations in random media in the white-noise regime, Ann. Appl. Probab., 19 (2009), pp. 318–346.

[7] P. Gérard, P. A. Markowich, N. J. Mauser, and F. Poupaud, Homogenization limits and Wigner transforms, Comm. Pure Appl. Math., 50 (1997), pp. 323–380.

[8] A. A. Gonoskov and I. A. Gonoskov, Suppression of reflection from the grid boundary in solving the time-dependent Schroedinger equation by split-step technique with fast fourier transform, Arxiv preprint 0607120v1, 2006.

[9] P.-L. Lions and T. Paul, Sur les mesures de Wigner, Rev. Mat. Iberoamericana, 9 (1993), pp. 553–618.

[10] R. F. O'Doherty and N. A. Anstey, Reflections on amplitudes, Geophysical Prospecting, 19, 430-458, 1971.

[11] K.E. Oughstun, Optimal pulse penetration in Rocard-Powles-Debye model dielectrics using the Brillouin precursor", IEEE Antennas and Propagation Society International Symposium, **4**, 4228–4231, (2004).

[12] G. Papanicolaou, L. Ryzhik, and K. Sølna, Statistical stability in time reversal, SIAM J. App. Math., 64(4) (2004), pp. 1133–1155.

[13] K. Sølna and G. Papanicolaou, Ray theory for a locally layered medium, Waves Random Media **10**, 2000, 155–202.

[14] F. Tappert, The parabolic approximation method, Wave propagation in underwater acoustics, Lecture Notes in Physics 70, Springer, (1977), pp. 224–287.